Journal of Molecular Catalysis A: Chemical 333 (2010) 6–10

Contents lists available at ScienceDirect

Journal of Molecular Catalysis A: Chemical

journal homepage: www.elsevier.com/locate/molcata

Editor's Choice paper

Electrocatalytic properties of platinum overgrown on various shapes of gold nanocrystals

Minkyu Min, Cheonghee Kim, Hyunjoo Lee*

Department of Chemical and Biomolecular Engineering, The Specialized Graduate School of Hydrogen & Fuel Cell, Yonsei University, Seoul 120-749, South Korea

ARTICLE INFO

Article history:
Received 10 August 2010
Received in revised form
28 September 2010
Accepted 28 September 2010
Available online 7 October 2010

Keywords:
Gold
Platinum
Composites
Shape
Electrocatalysts

ABSTRACT

Electrocatalytic properties of platinum layers overgrown on cubic, octahedral, and spherical gold nanocrystals were investigated. Electrochemically active surface area per unit mass of platinum was significantly different, depending on the shape of gold core nanocrystal. CO stripping results showed that binding of surface platinum atoms to CO was stronger than Pt black when platinum partially covered the gold surface. Au core@Pt shell composite nanoparticles generally demonstrated enhanced mass activity for methanol oxidation, formic acid oxidation, and oxygen reduction compared to Pt black; however, the extent of improvement differed considerably for the various shapes. Most notably, when specific activity was compared, platinum overgrown on octahedral gold crystals showed enhanced activity per unit area for formic acid oxidation and oxygen reduction. The shape of the underlying core nanocrystals significantly affects the electrocatalytic properties of surface platinum overgrown on the gold core.

1. Introduction

Recently, fuel cells have received tremendous attention for environmentally friendly energy utilization. Notably, platinum, which is the major catalyst in direct methanol fuel cells (DMFC) and proton exchange membrane fuel cells (PEMFC), has been actively investigated to improve the catalytic properties due to its high cost and limited reserves [1].

The activity, selectivity, and durability of a catalyst can be improved by combining more than two different types of metallic catalysts [2]. In particular, significant changes in the catalytic properties of platinum have been reported when platinum forms alloys with gold [3] or platinum nanoparticles are physically mixed with gold nanoparticles [4]. On the bimetallic surface of Au–Pt alloys, CO and OH adsorbed on Au sites participate in the catalyzed reaction that occurs on Pt sites, demonstrating enhanced bifunctional catalytic performance [5]. In the case of smaller gold nanoparticles deposited on platinum nanoparticles, the durability of the metallic catalysts was greatly enhanced for oxygen reduction. This improvement resulted from less oxidation of the platinum surface at high potentials, preventing surface poisoning from OH species [6]. Similarly, in examples where smaller platinum nanoparticles decorated gold nanoparticles, the platinum showed superior activity for oxygen reduction and formic acid oxidation [7–9]. When thin platinum layers are formed on gold nanotubes with nanoporous wall or nanoparticles, the platinum activity increased significantly for methanol oxidation [10–12].

The most usual way to prepare Au–Pt composite nanoparticles is to form a platinum shell on pre-made gold core nanoparticles by a chemical reduction method [13,14]. The gold nanoparticles are dispersed in a solution containing platinum precursors, which are reduced with chemical reducing agents to form Au core@Pt shell structure. Recent studies also demonstrated syntheses of dendritic platinum shells on gold cores using modified chemical reduction methods [15–20]. Their activities per unit mass of platinum were improved for methanol/formic acid oxidation and oxygen reduction [17–19].

Recently, we reported the synthesis of platinum shells overgrown on various shapes of gold nanocrystals [21]. In this study, electrocatalytic properties of Au@Pt nanoparticles of different geometries were evaluated. While most of previous studies for Au@Pt composite nanoparticles used undefined spherical gold cores, this study investigated how shaped gold cores affect the electrocatalytic properties of the platinum shell. Dispersion and surface structures of platinum shell were significantly different depending on the shape of the gold core. Their electrocatalytic activity and extent of poisoning were also affected.

2. Experimental

2.1. Synthesis of Au@Pt nanoparticles

Shaped Au@Pt nanoparticles were synthesized as reported previously [21]. First, different shapes of Au nanoparticles were

* Corresponding author. Tel.: +82 2 2123 5759; fax: +82 2 312 6401.
E-mail address: azhyun@yonsei.ac.kr (H. Lee).

1381-1169/$ – see front matter © 2010 Elsevier B.V. All rights reserved.
doi:10.1016/j.molcata.2010.09.020

prepared by adding 0.15 mL of different concentrations (1.7 mM for octahedra, 5 mM for cubes, and 17 mM for spheres) of $AgNO_3$ (99+%, Aldrich) to 5 mL of boiling 1,5-pentanediol (96%, Aldrich), followed by alternating additions of 200 μL of polyvinylpyrrolidone (PVP, MW 55,000, Aldrich; 0.15 M) and 200 μL of $HAuCl_4$ (99.9+%, Aldrich; 0.05 M) solution every 30 s. A total of 3 mL of each solution was added. The temperature of the mixture was maintained for 1 h at the boiling temperature of 1,5-pentanediol. Au nanoparticles in 1 mL of the resulting solution were washed several times with deionized (DI) water and re-dispersed in 4 mL of DI water. The suspension of Au nanoparticles (1 mL) was mixed with Pt salt solution prepared by adding 0.07 g K_2PtCl_4 (98%, Aldrich) into 2 mL of 0.2 M HCl and 98 mL of DI water. The atomic ratio of Pt/Au was 0.2 for Au(oct)@Pt, 0.2 for Au(cub)@Pt, 0.2 for Au(sph-p)@Pt and 0.6 for Au(sph-f)@Pt. Then, 10-fold excess of L-ascorbic acid (99+%, Aldrich), relative to Pt atoms, was added, and the total volume was diluted to 3 mL. The mixture was vigorously shaken and allowed to rest undisturbed overnight at room temperature (for Au octahedra, 50 °C). Finally, the synthesized Au@Pt nanoparticles were washed and dispersed in DI water.

2.2. Working electrode preparation

The aqueous dispersion of Au@Pt nanoparticles was sonicated and placed on a polished gold electrode with a 5-mm diameter. The same amount of platinum (2.35 μg, based on inductively coupled plasma elemental analysis) was loaded for each shape of Au@Pt nanoparticles. For platinum black (Aldrich), the electrode was prepared by dropping a dispersion of platinum black in 1:1 (v/v) water and isopropyl alcohol on a glassy carbon electrode with a diameter of 5 mm. Every electrode was dried and stored in a nitrogen atmosphere before measurements.

2.3. Electrochemical measurements

A three-electrode system was used for electrochemical measurements. An Ag/AgCl (saturated with NaCl solution) electrode was used as the reference electrode and a platinum wire was used as the counter electrode. Electrodes were connected to a VersaSTAT3 (Princeton Applied Research) potentiostat. Prior to all electrochemical measurements, CO annealing was performed to remove surface irregularities and to acquire reproducible results. The catalyst that was loaded on the working electrode was transferred to CO-saturated 0.1 M $HClO_4$ (70%, Aldrich). CO annealing was performed by cycling the electrode potential between −0.25 and 1.0 V (vs. Ag/AgCl) with a scan rate of 100 mV/s until identical voltammograms were obtained. Then, CO was bubbled for 5 additional minutes and N_2 was bubbled with the electrode potential at −0.2 V for 10 min. After that, CO stripping was performed by cycling the potential between −0.144 and 1.0 V with a scan rate of 50 mV/s. To calculate an electrochemical surface area (ESA), hydrogen adsorption/desorption voltammograms were acquired by cycling the potential at a scan rate of 50 mV/s from −0.144 to 0.59 V in N_2-saturated 0.1 M $HClO_4$. The ESA was determined from hydrogen desorption peak area above a double layer current in the range of −0.144 to 0.2 V by using 210 μC/Pt cm^2. The activity of methanol electro-oxidation was evaluated by cyclic voltammetry in a N_2-saturated solution of 0.5 M CH_3OH in 0.1 M $HClO_4$ with a scanning rate of 20 mV/s. Formic acid oxidation was performed in a N_2-saturated solution of 0.1 M HCOOH in 0.1 M $HClO_4$ with a scanning rate of 50 mV/s. Oxygen reduction was measured in O_2-saturated 0.1 M $HClO_4$ with a scanning rate of 50 mV/s, which was obtained by bubbling ultra high-purity O_2 gas (99.995%) for at least 20 min.

2.4. Characterizations

TEM images were obtained with a JEOL 2100. X-ray photoelectron spectroscopy (XPS) data were acquired using a SIGMA probe (ThermoVG) equipped with a monochromatic Al Kα X-ray source (15 kV, 100 W). The binding energy was calculated with reference to the maximum intensity of the C1s signal at 285.0 eV. Elemental analysis was performed with inductively coupled plasma (ICP; IRIS Intrepid II, Thermo Elemental).

3. Results and discussions

Platinum was overgrown on differently shaped gold nanocrystals: octahedra, cubes, and spheres. Fig. 1 shows TEM images of Au(oct)@Pt, Au(cub)@Pt, and Au(sph)@Pt, where platinum was overgrown on octahedral, cubic, and spherical Au nanocrystals, respectively. Au(sph-p)@Pt denotes partially covered gold cores while Au(sph-f)@Pt represents fully covered cores. Fig. 1(c) and (d) shows different thicknesses of the Pt shell on spherical Au nanocrystals. As demonstrated in the inset of Fig. 1(c), the platinum was heteroepitaxially overgrown on Au crystals. Platinum grew on the vertexes of Au octahedra while it grew on facets of Au cubes. As shown in Ref. [21], platinum overgrew selectively on the Au(1 0 0) surface, replacing residual Ag located on Au(1 0 0) surface.

Fig. 2 shows XPS Pt 4f and Au 4f peaks for various Au@Pt nanoparticles. Considering that XPS generally collects information up to five atomic layers below the surface, the presence of Au peaks – even for Au(sph-f)@Pt, where platinum fully covers the surface of Au sphere with a thickness of ~13 nm – implies that the platinum shell is dendritic. The peaks in Fig. 2 were normalized to the maximum intensity of Au 4f peak for each sample. The ratio of Pt/Au on the surface was compared by measuring the peak areas. The Pt/Au peak area ratio was 1.4 for Au(oct)@Pt, 1.8 for Au(sph-p)@Pt, 2.6 for Au(cub)@Pt, and 3.4 for Au(sph-f)@Pt. The location of Pt 4f peaks was 74.7 and 71.4 eV for Pt black, as denoted by straight line in Fig. 2. Pt 4f peaks for all Au@Pt nanoparticles were negatively shifted, with reduced binding energy relative to Pt black, implying that electron transfer occurs from Au to Pt as reported previously [11].

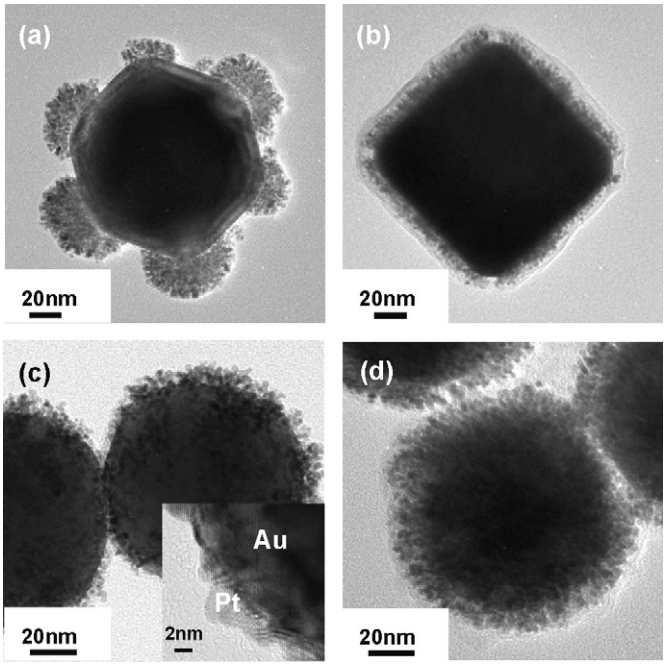

Fig. 1. TEM images of (a) Au(oct)@Pt, (b) Au(cub)@Pt, (c) Au(sph-p)@Pt, and (d) Au(sph-f)@Pt. The inset of (c) shows a high resolution TEM image of Au(Sph-p)@Pt.

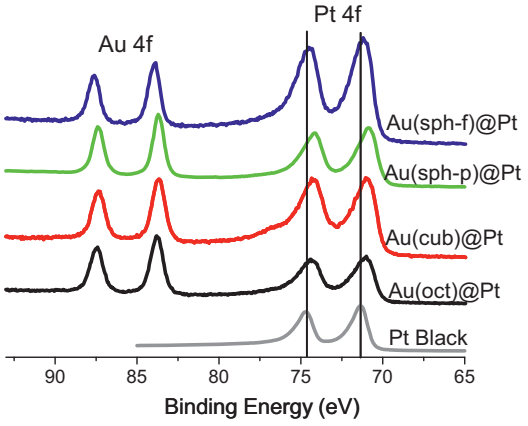

Fig. 2. X-ray photoelectron spectra of Au@Pt nanoparticles and Pt black.

The residual Ag on the surface of Au@Pt nanoparticles may affect the electrocatalytic properties. The Ag/Pt peak area ratio was measured as 0 for Au(oct)@Pt, 0.05 for Au(cub)@Pt, 0.10 for Au(sph-p)@Pt, and 0.10 for Au(sph-f)@Pt. As explained later, no trends in electrocatalytic measurements were observed that correlated to the amount of residual Ag. Even for Au(sph-p)@Pt and Au(sph-f)@Pt with the same ratio of Ag/Pt, their electrocatalytic properties were very different. The effect of residual Ag on electrocatalytic properties seems to be negligible.

The various Au@Pt nanoparticles were used as electrocatalysts. Au nanocrystals themselves did not show any activity in electrocatalytic reactions. CO annealing was performed for all Au@Pt nanoparticles and Pt black prior to electrocatalytic measurement to remove surface irregularities and to obtain reproducible results [22]. CO annealing was performed by cycling the electrode potential between −0.25 and 1.0 V with a scan rate of 100 mV/s until identical voltammograms were obtained. H adsorption/desorption cyclic voltammograms were obtained with a scan rate of 50 mV/s in 0.1 M $HClO_4$, as shown in Fig. 3. The ESA in Table 1 was determined from the H desorption curves of Fig. 3. While the platinum nanoparticles overgrown on various shapes of gold nanocrystals had the similar domain size of 2–3 nm, how the platinum nanoparticles are connected seems to be different. Platinum nanoparticles overgrown on gold octahedra looked more condensed, but platinum nanoparticles overgrown on gold cubes or partially overgrown on gold sphere looked more exposed. Platinum overgrown on Au octahedra had the smallest ESA per unit mass while platinum on Au cubes or partially overgrown on Au spheres had a greater ESA per unit mass. The overgrowth concentrated on the smaller area of vertexes of octahedral nanocrystals while platinum overgrew on facets of cube or surfaces of spheres.

Table 1
Electrochemically active surface area (ESA) of Au@Pt nanoparticles and Pt black measured from hydrogen desorption.

	ESA (m^2/g)
Au(oct)@Pt	8.5
Au(cub)@Pt	23.4
Au(sph-p)@Pt	21.3
Au(sph-f)@Pt	14.9
Pt black	8.1

CO stripping was performed to estimate the interactions between reactants and platinum surface atoms. CO was adsorbed on platinum surfaces, and CO stripping was performed between −0.144 and 1.0 V with a scan rate of 50 mV/s. Full CO adsorption was confirmed by the lack of H desorption peak between −0.144 and 0.2 V. Fig. 4 shows CO stripping peaks in the range of 0.3–0.8 V. As the stripping peak is located at a higher potential, CO is bound to the platinum surface atoms stronger. The position of the peak potentials were 0.58 V for Au(sph-f)@Pt, 0.59 V for Pt black, 0.60 V for Au(cub)@Pt, 0.64 V for Au(oct)@Pt, and 0.64 V for Au(sph-p)@Pt. When platinum was locally overgrown on gold surfaces, such as Au(oct)@Pt and Au(sph-p)@Pt, the interaction between CO and platinum atoms was stronger. The stronger CO–Pt bonding for partially covered platinum deposited on the gold surface was also reported previously [23]. Platinum fully grown on Au spheres had even lower peak potential than Pt black. Additionally, all the Au@Pt nanoparticles have broader CO stripping peaks than Pt black. Au@Pt nanoparticles seem to have less uniform active sites than Pt black.

The activity for methanol oxidation was tested in a solution containing 0.1 M $HClO_4$ and 0.5 M CH_3OH with a scan rate of 20 mV/s, as displayed in Fig. 5. Au(sph-f)@Pt showed the highest mass activity while the activity of Au(oct)@Pt was as low as Pt black. Au(oct)@Pt showed the lowest mass activity due to the smallest surface area and strong binding to CO, which acts as surface poison during methanol oxidation. In spite of their large surface areas, Au(cub)@Pt and Au(sph-p)@Pt had medium mass activity due to strong binding to CO. The methanol oxidation activity was the highest for Au(sph-f)@Pt because it has relatively large surface area and weak binding to CO, enabling less surface poisoning. When specific activities (activity per unit surface area) were compared, however, only Au(sph-f)@Pt had a higher specific activity (3.6 mA/cm^2) than Pt black (3.3 mA/cm^2). The specific activity was 2.9 mA/cm^2 for Au(oct)@Pt, 2.7 mA/cm^2 for Au(cub)@Pt, and 2.1 mA/cm^2 for Au(sph-p)@Pt. On the other hand, the location of peak potentials in the forward scan was also compared. Compared to 0.57 V for Pt black, Au@Pt nanoparticles showed positive shift to 0.59 V for

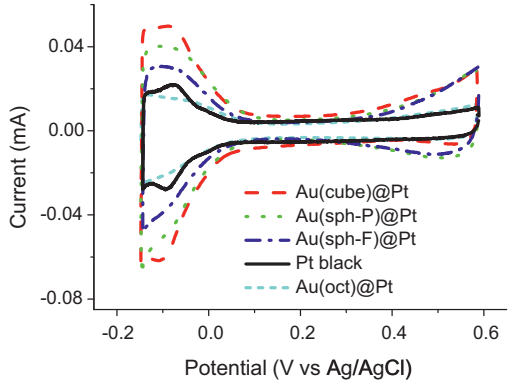

Fig. 3. Cyclic voltammograms during H adsorption/desorption by Au@Pt nanoparticles and Pt black measured with a scan rate of 50 mV/s in 0.1 M $HClO_4$ solution. The mass of Pt in each sample was 2.35 μg.

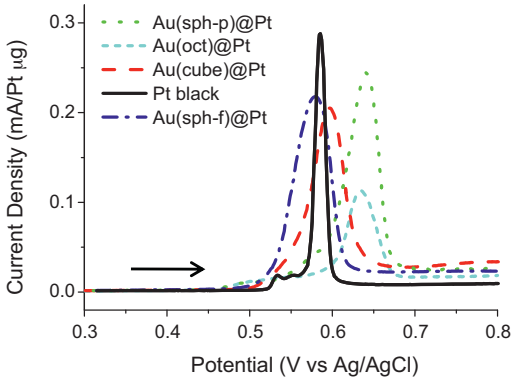

Fig. 4. Voltammograms displaying CO stripping by Au@Pt nanoparticles and Pt black in 0.1 M $HClO_4$ after CO annealing process. The scan rate was 50 mV/s.

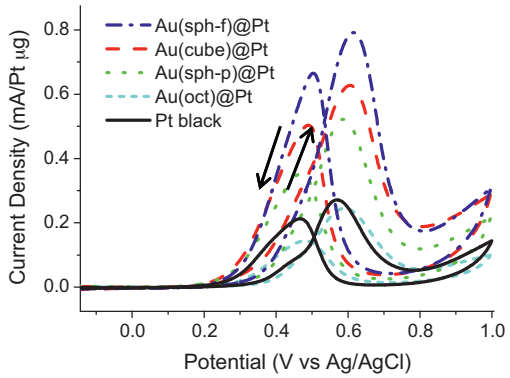

Fig. 5. Cyclic voltammograms during methanol oxidation by Au@Pt nanoparticles and Pt black in a solution of 0.1 M $HClO_4$ and 0.5 M CH_3OH at room temperature. The scan rate was 20 mV/s.

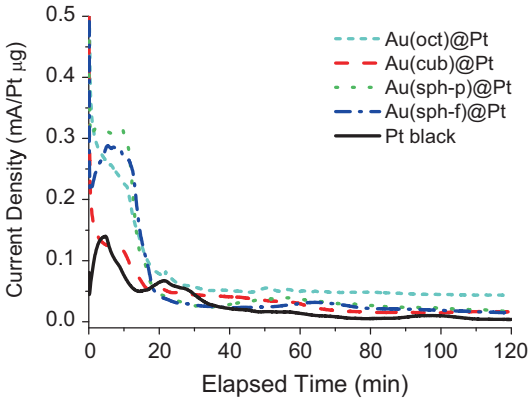

Fig. 7. Chronoamperometry results by Au@Pt nanoparticles and Pt black. 0.1 M of formic acid was oxidized in 0.1 M $HClO_4$ solution at 0.3 V for 2 h at room temperature.

Au(oct)@Pt, 0.59 V for Au(sph-p)@Pt, 0.61 V for Au(cub)@Pt and 0.62 V for Au(sph-f)@Pt. Competition between CO adsorption and OH adsorption occurs in methanol oxidation, and the methanol oxidation peak in the forward scan started to decrease because adsorbed OH poisoned the platinum surface at high potentials [24]. Higher peak potentials of Au@Pt nanoparticles indicate that Au@Pt nanoparticles have more resistance to formation of poisoning oxide species. The ratio of the forward peak current density (I_f) and the reverse peak current density (I_r) was compared. I_f/I_r ratio was 1.2 for Au(sph-f)@Pt, 1.3 for Au(cub)@Pt, 1.5 for Au(sph-p)@Pt, 1.7 for Au(oct)@Pt, and 1.3 for Pt black, respectively. A low I_f/I_r ratio indicates poor electro-oxidation of methanol to carbon dioxide during the forward scan, and excessive accumulation of carbonaceous intermediates on the catalyst surface [25,26]. Au(oct)@Pt showed a slightly higher I_f/I_r ratio compared to other catalysts.

Fig. 6 shows the results for formic acid oxidation performed in a solution containing 0.1 M $HClO_4$ and 0.1 M HCOOH with a scan rate of 50 mV/s. Electrocatalytic oxidation of formic acid on platinum generally follows two reaction pathways: dehydrogenation ($HCOOH \rightarrow H_2 + CO_2$) or dehydration ($HCOOH \rightarrow H_2O + CO$). Because dehydration pathway generates the surface poisoning species of CO during the reaction, the activity decreases as the reaction proceeds with the dehydration pathway. The peak at ~0.34 V in the forward scan represents the peak associated with direct dehydrogenation oxidation, and the peak at ~0.63 V in the forward scan represents oxidation of CO_{ads} adsorbed on the platinum surface [9]. In the case of Pt black, very little direct dehydrogenation was observed in the forward scan, and a large indirect dehydration peak appeared due to CO_{ads} oxidation. On the other hand, all Au@Pt nanoparticles show large dehydrogenation peak indicating that direct oxidation occurred much more than Pt black. Notably, Au(oct)@Pt had a very small dehydration peak, implying that most formic acid oxidation occurs by direct oxidation following the dehydrogenation pathway. When specific activities were compared, the intensity of the dehydrogenation peak in the forward scan was greatest for Au(oct)@Pt (4.7 mA/cm^2). The peak intensity was 2.5 mA/cm^2 for Au(cub)@Pt, 2.4 mA/cm^2 for Au(sph-p)@Pt, 1.9 mA/cm^2 for Au(sph-f)@Pt, and 0.5 mA/cm^2 for Pt black, respectively. It was reported that formic acid oxidation rates are enhanced by a factor of 20 when platinum is deposited on Au(1 1 1) compared to Pt(1 1 1) [27]. The underlying shape of the Au octahedral nanocrystals might cause the enhanced activity for formic acid oxidation. The long-term stability of Au@Pt nanoparticles was also tested for formic acid oxidation at 0.3 V. As shown in Fig. 7, Au(oct)@Pt showed the best current density of 0.042 mA/μg while Pt black showed very low current density of 0.004 mA/μg after 2 h of operation. The current density was 0.016 mA/μg for Au(cub)@Pt, 0.017 mA/μg for Au(sph-p)@Pt, and 0.014 mA/μg for Au(sph-f)@Pt. Au@Pt nanoparticles still showed enhanced current density compared to Pt black after extended hours of operation.

The cathodic reaction of fuel cells was also tested for various Au@Pt nanoparticles and Pt black. Oxygen reduction was measured in O_2-saturated 0.1 M $HClO_4$ with a scanning rate of 50 mV/s by decreasing the potential from 1.0 V as shown in Fig. 8. Relative to Pt black, the onset potential where oxygen reduction starts to occur was higher for Au@Pt nanoparticles, and the peak intensity per unit mass of platinum was also higher for Au@Pt nanoparticles. However, when specific activities were compared, Au(oct)@Pt showed the highest activity (0.69 mA/cm^2) and Au(sph-f)@Pt exhibited the

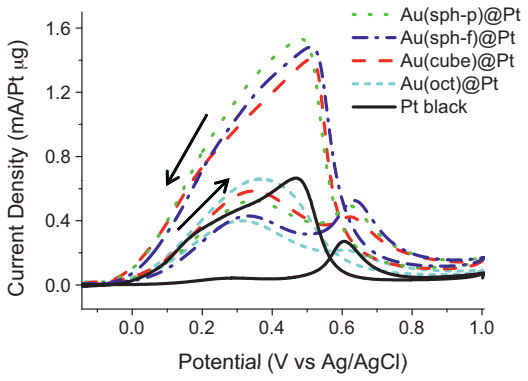

Fig. 6. Cyclic voltammograms during formic acid oxidation by Au@Pt nanoparticles and Pt black in a solution of 0.1 M $HClO_4$ and 0.1 M HCOOH at room temperature. The scan rate was 50 mV/s.

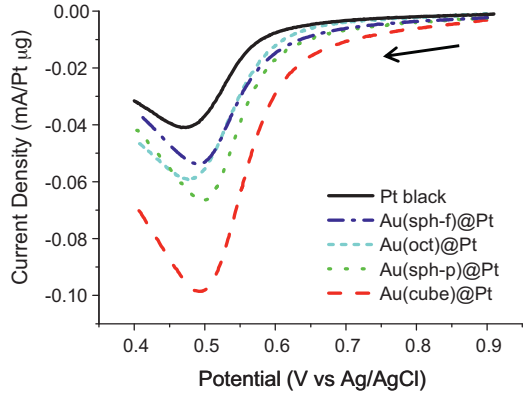

Fig. 8. Cathodic sweep showing oxygen reduction by Au@Pt nanoparticles and Pt black in O_2-saturated 0.1 M $HClO_4$ solution at room temperature. The scan rate was 50 mV/s.

lowest activity (0.24 mA/cm^2); the specific activity of Pt black was 0.50 mA/cm^2. A recent study demonstrated that oxygen reduction occurs more on Pt(1 1 1) domains while methanol oxidation occurs more on stepped sites [28]. Enhanced oxygen reduction on Au(oct)@Pt might be attributed to more Pt(1 1 1) surfaces formed on Au(oct)@Pt nanoparticles. Similarly, more stepped sites on Au(sph-f)@Pt might cause the enhanced methanol oxidation.

4. Conclusions

Electrocatalytic properties of platinum overgrown on cubic, octahedral and spherical gold nanocrystals were investigated. The electrochemically active surface area per unit mass of platinum was significantly different based on the shape of underlying gold core nanocrystal. When platinum partially covered the gold surface, such as Au(oct)@Pt or Au(sph-p)@Pt, the interactions of the platinum surface with CO was much stronger. Contrastingly, Au(cub)@Pt and Au(sph-f)@Pt showed a binding strength to CO that was similar to Pt black. Au(sph-f)@Pt, with a relatively large surface area and weak interactions with CO, showed the highest mass activity and specific activity for methanol oxidation. For formic acid oxidation, all the Au@Pt nanoparticles followed direct dehydrogenation pathways more, showing much less poisoning than Pt black. Au(cub)@Pt had the highest mass activity for oxygen reduction. However, when the specific activities were compared, Au(oct)@Pt showed the highest activity, implying that more Pt(1 1 1) is present. The activity for electrocatalytic reactions and the extent of surface poisoning of the overgrown platinum surface were significantly affected by the shape of underlying gold core crystals.

Acknowledgment

This work was supported by the Korea Research Foundation Grant funded by the Korean Government (MOEHRD) (KRF-2008-313-D00196).

References

[1] V. Mazumder, Y. Lee, S.H. Sun, Adv. Funct. Mater. 20 (2010) 1224–1231.
[2] E. Nikolla, J. Schwank, S. Linic, J. Catal. 250 (2007) 85–93.
[3] B. Ballarin, M. Gazzano, E. Scavetta, D. Tonelli, J. Phys. Chem. C 113 (2009) 15148–15154.
[4] L. Wang, Y. Yamauchi, Chem. Mater. 21 (2009) 3562–3569.
[5] J. Luo, P.N. Njoki, Y. Lin, D. Mott, L.Y. Wang, C.J. Zhong, Langmuir 22 (2006) 2892–2898.
[6] J. Zhang, K. Sasaki, E. Sutter, R.R. Adzic, Science 315 (2007) 220–222.
[7] S.J. Guo, S.J. Dong, E.K. Wang, J. Phys. Chem. C 113 (2009) 5485–5492.
[8] N. Kristian, Y.S. Yan, X. Wang, Chem. Commun. (2008) 353–355.
[9] S. Zhang, Y.Y. Shao, G.P. Yin, Y.H. Lin, Angew. Chem. Int. Ed. 49 (2010) 2211–2214.
[10] T.Y. Shin, S.H. Yoo, S. Park, Chem. Mater. 20 (2008) 5682–5686.
[11] J.H. Zeng, J. Yang, J.Y. Lee, W.J. Zhou, J. Phys. Chem. B 110 (2006) 24606–24611.
[12] D. Zhao, B.Q. Xu, Angew. Chem. Int. Ed. 45 (2006) 4955–4959.
[13] N. Kristian, X. Wang, Electrochem. Commun. 10 (2008) 12–15.
[14] L. Yang, J.H. Chen, X.X. Zhong, K.Z. Cui, Y. Xu, Y.F. Kuang, Colloids Surf. A 295 (2007) 21–26.
[15] H. Ataee-Esfahani, L. Wang, Y. Yamauchi, Chem. Commun. 46 (2010) 3684–3686.
[16] L.L. Feng, X.C. Wu, L.R. Ren, Y.J. Xiang, W.W. He, K. Zhang, W.Y. Zhou, S.S. Xie, Chem. Eur. J. 14 (2008) 9764–9771.
[17] H.P. Liang, T.G.J. Jones, N.S. Lawrence, L. Jiang, J.S. Barnard, J. Phys. Chem. C 112 (2008) 4327–4332.
[18] Z.M. Peng, H. Yang, Nano Res. 2 (2009) 406–415.
[19] S.Y. Wang, N. Kristian, S.P. Jiang, X. Wang, Nanotechnology 20 (2009), 025605.
[20] S.G. Zhou, K. McIlwrath, G. Jackson, B. Eichhorn, J. Am. Chem. Soc. 128 (2006) 1780–1781.
[21] M. Min, C. Kim, Y.I. Yang, J. Yi, H. Lee, Phys. Chem. Chem. Phys. 11 (2009) 9759–9765.
[22] S. Kumar, S.Z. Zou, Langmuir 23 (2007) 7365–7371.
[23] B.C. Du, Y.Y. Tong, J. Phys. Chem. B 109 (2005) 17775–17780.
[24] T. Iwasita, X.H. Xia, H.D. Liess, W. Vielstich, J. Phys. Chem. B 101 (1997) 7542–7547.
[25] J.J. Wu, H.L. Tang, M. Pan, Z.H. Wan, W.T. Ma, Electrochim. Acta 54 (2009) 1473–1477.
[26] R. Manoharan, J.B. Goodenough, J. Mater. Chem. 2 (1992) 875–887.
[27] J. Kim, C. Jung, C.K. Rhee, T.H. Lim, Langmuir 23 (2007) 10831–10836.
[28] S.W. Lee, S. Chen, J. Suntivich, K. Sasaki, R.R. Adzic, Y. Shao-Horn, J. Phys. Chem. Lett. 1 (2010) 1316–1320.